

Impedance technology reveals correlations between cytotoxicity and lipophilicity of mono and bimetallic phosphine complexes

P. Fonteh^a, A. Elkhadir^b, B. Omondi^b, I. Guzei^c, J. Darkwa^b, D. Meyer^{a, d}✉

^aDepartment of Biochemistry, University of Pretoria, Pretoria 0002, South Africa

^bDepartment of Chemistry, University of Johannesburg, Auckland Park, Johannesburg 2006, South Africa

^cDepartment of Chemistry, University of Wisconsin-Madison, 1101 University Ave, Madison, WI 53706, USA.

^dPresent address: Department of Biochemistry, University of Johannesburg, P.O. Box 524, Auckland Park, 2006

✉ Email: dmeyer@uj.ac.za, Tel: + 27-11-559-2825, Fax: +27-11-559-2307

Abstract

Label free impedance technology enables the monitoring of cell response patterns posttreatment with drugs or other chemicals. Using this technology, a correlation between the lipophilicity of metal complexes and the degree of cytotoxicity was observed. Au(L1)Cl (**1**), AuPd(L1)(SC₄H₈)Cl₃ (**1a**) and Au(L2)Cl (**2**) (L1 = (diphenylphosphino-2-pyridine); L2 = 2-(2-(diphenylphosphino)ethyl)-pyridine) were synthesised, *in silico* drug-likeness and structure activity relationship (SAR) monitored using impedance technology. Dose dependent changes in cytotoxicity were observed for the metal complexes resulting in IC_{50s} of 12.5±2.5, 18.3±8.3 and 16.9±0.5 µM for **1**, **1a** and **2** respectively in an endpoint assay. When a real time impedance assay was used, dose-dependent responses depicting patterns that suggested slower uptake (at a toxic 20 µM) and faster recovery of the cells (at the less toxic 10 µM) of the bimetallic complex (**1a**) compared to the monometallic complexes (**1** and **2**) was observed. These data agreed with the ADMET findings of lower aqueous solubility of **1a** and non ideal lipophilicity (AlogP98 of 6.55) over more water soluble **1** and **2** with ideal lipophilicity (4.91 and 5.03 respectively) values. The additional coordination of a Pd atom to the nitrogen atom of a pyridine ring, the sulfur atom of a tetrahydrothiophene (THT) moiety and two chlorine atoms in **1a** could be contributing to the observed differences when compared to the monometallic complexes. This report presents impedance technology as a means of

correlating drug-likeness of lipophilic phosphine complexes containing similar backbone structures and could prove valuable in filtering drug-like compounds in a drug discovery project.

Keywords: impedance; uptake; recovery; lipophilicity; phosphine gold complexes

1. INTRODUCTION

The study of drug-like or absorption, distribution, metabolism, excretion and toxicity (ADMET) properties of new chemicals early in drug discovery has gained significant importance over the last decade due to the high rate of late drug failures during clinical trials (Hamid et al, 2004), in addition to other adverse effects. *In silico* prediction models provides insight into potential toxicity and can significantly shorten the drug discovery time line (Lobell and Sivarajah 2003). It is however important that these data be complemented with *in vitro* experimental studies because of the physiological relevance of the latter. This is one of the main reasons why cell-based assays continue to grow in importance in drug discovery especially since the data can be extrapolated to pharmacological endpoints (McGuinness 2007).

Until recently, toxicity has largely been tested using end point assays which unfortunately are not dynamic and focus on measuring just one parameter (Xing et al, 2006). These end point assays usually include the use of a label for monitoring various cellular functions that are then detected using methods such as optical absorbance, fluorescence, luminescence or radioisotopic techniques (Solly et al, 2004). The labels sometimes interfere with test compounds, involve time consuming labelling and wash steps and could potentially affect physiological conditions in cell culture (Solly et al, 2004). The use of label-free technology has therefore been emerging as a way of identifying drug-like compounds. One such methodology is electrical detection based on cell substrate impedance measurement (Giaever and Keese 1984). The principle of the technique is based on the fact that most non hematopoietic cells attach firmly to the ideal substrate while injured cells will round up and finally detach, which is associated with cell death (Kepp et al, 2011). By measuring the impedance of the surface occupied by the cells, an indirect indicator of viability (Solly et al, 2004; Atienza et al, 2005; Xing et al, 2005) or cytotoxicity (Boyd et al, 2008; Xing et al, 2005; Xing et al, 2006) is obtained. The advantages of impedance technology makes the data relevant in complementing these end point assays by providing additional information on cellular parameters such as cytotoxicity, cell proliferation, cell recovery, and cell response patterns (Xing et al,

2005) in real time. This technique is therefore ideal for determining drug-like properties of potential drugs and was further used here to correlate structure, uptake, toxicity and lipophilicity profiles.

Gold-based compounds have been widely exploited for anti-cancer activity (Nobili et al, 2010; Sun and Che 2009; Monim-ul-Mehboob et al, 2013) as well as for inhibition of various pathogens such as the human immunodeficiency virus (HIV) (Shapiro and Masci 1996; Fonteh et al, 2009; Fonteh et al, 2011). One limitation of the earliest anti-HIV gold-based drugs such as the injectable gold compound, aurothioglucose and its metabolites was the fact that they could not be taken up by cells due to poor lipophilicity (Okada et al, 1993; Zhang et al, 1995). Aurothioglucose unlike auranofin lacks a phosphine moiety; which is known to confer the lipophilic property and hence oral availability of the latter group (Shaw III et al, 1994). The addition of a second similar (homo-bimetal) or different metal (hetero-bimetal) has shown improved activity due to synergism between the metals or dual biological activity since each metal maintains its chemical identity with the resultant inhibition of multiple sites (Rupesh et al, 2006). Palladium is one such metal which has been considered in bimetallic synthesis since compounds of this metal have biological properties such as anti-cancer activity (Ray et al, 2007; Wang et al, 2011). The addition of a second metal however affects lipophilicity and hence drug-likeness of the complexes.

Lipophilicity is used to assess biological parameters relevant to drug action such as lipid solubility, tissue distribution, receptor binding, cellular uptake, metabolism and bioavailability (Ghose et al, 1998). In this study, one novel bimetallic complex (**1a**) and two monometallic gold-based phosphine complexes (**1** and **2**) were synthesised and characterised. Cytotoxicity effects of the compounds was determined on TZM-bl cells using the 3-(4,5-dimethylthiazol-2-yl)-2,5-diphenyltetrazolium bromide (MTT) tetrazolium dye. The impedance technology of the real time cell electronic sensing (RT-CESTM, ACEA Biosciences Inc., San Diego, USA) device was used to further complement MTT findings while lipophilicity predictions were done using the ADMET prediction protocol in DS[®]. The cell response patterns with regards to compound toxicity (both MTT and RT-CESTM) as well as uptake and recovery after uptake in the RT-CESTM assay were shown to correlate with the lipophilicity levels obtained from *in silico* ADMET predictions. These findings demonstrate the ability of impedance technology in correlating uptake of chemicals or recovery of cells after treatment with lipophilic phosphine gold monometallic and bimetallic

gold-palladium complexes. These findings are useful in complementing ADMET studies and could aid in reducing the attrition rate for these types of complexes or others in a drug discovery study.

2. Materials and Methods

For the synthetic processes, all manipulations were carried out under argon by standard Schlenk techniques. All Solvents were of analytical grade and were dried using a Braun MB SPS-800 drying solvent system. Diphenylphosphino-2-pyridine (**L1**) and 2-(2-(diphenylphosphino)ethyl)pyridine (**L2**) were purchased from Sigma-Aldrich and were used as received.

The gold and palladium starting materials, chloroauric acid $\text{H}[\text{AuCl}_4]$ and palladium dichloride $[\text{PdCl}_2]_n$, were purchased from South Africa Precious Metals. The starting materials gold(tetrahydrothiophene)chloride $[\text{Au}(\text{THT})\text{Cl}]$ (Uson et al, 1989) and *bis*(acetonitrile)-dichloropalladium(II) $[\text{Pd}(\text{NCMe})_2\text{Cl}_2]$ (Rülke et al, 1990) were synthesized following literature procedures. Diphenylphosphino-2-pyridylgold(I) chloride (**1**) and 2-(2-(diphenylphosphino)ethyl)pyridylgold(I) chloride (**2**) were prepared using the method by Calhorda and colleagues (Calhorda et al, 2010) and hence there is no need for discussion of the spectral data.

2.1 Instrumentation

^1H NMR and $^{13}\text{C}\{^1\text{H}\}$ NMR spectra were recorded in chloroform-*d* (CDCl_3) on a Varian Gemini 2000 instrument (at 300 MHz for ^1H NMR, at 75.46 MHz for $^{13}\text{C}\{^1\text{H}\}$ NMR and at 121.49 MHz for $^{31}\text{P}\{^1\text{H}\}$ NMR) and on a Bruker Ultrashield 400 instrument (at 400 MHz for ^1H NMR, at 100.61 MHz for $^{13}\text{C}\{^1\text{H}\}$ NMR and at 161.97 MHz for $^{31}\text{P}\{^1\text{H}\}$ NMR) at room temperature. ^1H and $^{13}\text{C}\{^1\text{H}\}$ NMR chemical shifts were referenced to the residual signals of the protons or carbons of the NMR solvents and are quoted in δ (ppm): CDCl_3 at 7.24 and 77.00 ppm for ^1H and $^{13}\text{C}\{^1\text{H}\}$ NMR spectra respectively. Coupling constants are measured in Hertz (Hz). Elemental analyses were performed on a Vario Elementar III microcube CHNS analyzer at Rhodes University, South Africa.

2.2.1 Synthesis of palladium(tetrahydrothiophene)[(diphenylphosphino-2-pyridyl)]AuCl chloride (**1a**):

To a chloroform solution (10 mL) of diphenylphosphino-2-pyridine (0.05 g, 0.10 mmol) was added $[\text{Au}(\text{THT})\text{Cl}]$ (0.03 g, 0.10 mmol). The solution was stirred for 20 min before $[\text{Pd}(\text{NCMe})_2\text{Cl}_2]$ (0.01 g,

0.05 mmol) was added and stirring continued for a further 30 min. Hexane (10 mL) was added to precipitate the crude product, which was filtered and dried *in vacuo*. Analytically pure product was obtained from re-crystallization of the crude product in a chloroform-hexane mixture to afford bright yellowish-orange crystals. A yield of 80% (0.06 g) was obtained. ^1H NMR (CDCl_3): δ 1.94 (s, 2H) 2.31 (s, 2H), 2.77 (s, 2H), 3.61 (s, 2H), 7.35 (t, 1H), 7.46 (m, 4H), 7.56 (m, 6H), 7.69 (q, 1H, $J = 5.6, 7.6$ & 8.0 Hz), 7.79 (t, 1H), 9.39 (d, 1H, $J = 5.2$ Hz). $^{31}\text{P}\{^1\text{H}\}$ (CDCl_3) 37.54 (s, 1P). $^{13}\text{C}\{^1\text{H}\}$ NMR (CDCl_3) 29.5; 30.1; 37.7; 38.5; 126.9; 127.1; 127.8; 129.3; 132.3, 132.4, 132.7, 132.8; 134.2, 134.4; 138.1; 155.2, 155.3; 156.3. Anal. Calcd. for $\text{C}_{21}\text{H}_{22}\text{PAuCl}_3\text{NPdS}\cdot\text{CHCl}_3$, C, 30.01; H, 2.63; N, 1.59; S, 3.64%. Found: C, 30.07; H, 2.52; N, 1.47; S, 3.64%.

2.3 X-ray structure determination

2.3.1 Data collection

A crystal of **2** (as a representative compound) of dimensions $0.32 \times 0.06 \times 0.02 \text{ mm}^{-3}$ was selected and glued on to the tip of a glass fibre. The crystal was then mounted in a stream of cold nitrogen at 100(1) K and centred in the X-ray beam using a video camera. The crystal evaluation and data collection were performed on a Bruker APEXII diffractometer with Mo $\text{K}\alpha$ ($\lambda = 0.71073 \text{ \AA}$) radiation and the diffractometer to crystal distance of 4.00 cm. The initial cell matrix was obtained from three series of scans at different starting angles. Each series consisted of 12 frames collected at intervals of 0.5° in a 6° range about with the exposure time of 10 seconds per frame. The reflections were successfully indexed by an automated indexing routine built in the APEXII program suite (Bruker 2009). The final cell constants were calculated from a set of 6460 strong reflections from the actual data collection.

The data were collected by using the full sphere data collection routine to survey the reciprocal space to the extent of a full sphere to a resolution of 0.75 \AA . A total of 4426 data were harvested by collecting 1109 frames at intervals of 0.5° scans in 6° and φ with exposure times of 15 sec per frame. These highly redundant datasets were corrected for Lorentz and polarization effects. The absorption correction was based on fitting a function to the empirical transmission surface as sampled by multiple equivalent measurements (Bruker 2009).

2.2 .2 Structure solution and refinement

The systematic absences in the diffraction data were uniquely consistent for the space group $P2_1/c$ that yielded chemically reasonable and computationally stable results of refinement. A successful solution by the direct methods of SIR92 (Altomare et al, 1993) provided all non-hydrogen atoms from the E-map. All non-hydrogen atoms were refined with anisotropic displacement coefficients. All hydrogen atoms except those on the solvent water molecules were included in the structure factor calculation at idealized positions and were allowed to ride on the neighbouring atoms with relative isotropic displacement coefficients. The final least-squares refinement of 205 parameters against 4286 data resulted in residuals R (based on F2 for $I \geq 2\sigma$) and wR (based on F2 for all data) of 0.0198 and 0.0515, respectively. The final difference Fourier map was featureless. The molecular diagrams are drawn with 50% probability ellipsoids (Palatinus and Chapuis 2007; Farrugia 1999; Farrugia 1997; Sheldrick 2008).

2.4 Culturing of TZM-bl cells

The TZM-bl cell line from Dr. John C. Kappes, Dr. Xiaoyun Wu and Tranzyme Inc, (Takeuchi et al, 2008; Wei et al, 2002; Derdeyn et al, 2000; Platt et al, 1998) was used in determining toxicity and proliferation. This is an adherent HeLa cell line engineered to stably express CD4, CXCR4 and CCR5 and containing reporter genes controlled by the HIV-1 promoter enabling HIV-1 infectivity determination. These cells are a model cell line for testing HIV infectivity and was used because of our previous work with HIV and also because we aimed in a separate study to determine the effect of the compounds on HIV infectivity.

The cells were sub-cultured in T-75 tissue culture flasks (NuncTM, Roskilde, Denmark) with approximately 10^6 cells in 15 mL of complete Dulbecco's Modified Eagle Medium (DMEM) with L-glutamine (Sigma Aldrich, Missouri, USA) containing sodium pyruvate (100 mM, Thermo Scientific, HyClone®, UT, USA), hepes buffer (1M, Gibco BRL Life Technologies, Grand Island, USA), sodium bicarbonate (3.70 g/L, Merck, Wadeville, RSA), antibiotics (50 µg/mL gentamycin sulphate, Sigma Aldrich, Missouri, USA) and 10% (v/v) heat inactivated fetal calf serum (Thermo Scientific, HyClone®, UT, USA). Sub-culturing was done every two or three days when confluency (surface area of the culture flask occupied by cells) was about 90%. Cell culture conditions for the bioassays (MTT and impedance), which included cell number, media volume and incubation time, were established through titration

experiments on the RT-CESTM analyser. The pre-determined conditions were maintained for both bioassays since a similarity in the efficiency for viable cell count has been reported for the two (Xing et al, 2006).

2.5 Cytotoxicity determination with MTT

To obtain cells in the exponential phase of growth, 100 μL of TZM-bl cells at 2×10^5 cells/mL in complete DMEM medium were plated in 96 well tissue culture plates to a final volume of 200 μL . The cells were allowed to adhere and reach confluency (after 22-24 h) in a 5% CO_2 incubator (37 $^\circ\text{C}$, 95% humidity). Compound stocks were dissolved in DMSO and further diluted with culture medium to a final DMSO concentration $\leq 0.5\%$ (v/v). The concentrations of the compounds attained in wells ranged from 0.8-100 μM (250 μL final volume). An untreated control sample contained cells and culture medium only while a blank control sample contained medium only. The cells were further incubated for 48 h (37 $^\circ\text{C}$, 90% humidity, 5% CO_2) after which 190 μL of spent medium was discarded and replaced with 140 μL of complete medium and 20 μL of 5 mg/mL MTT. Colour development was analysed after 2 h following solubilisation of the MTT formazan product using acidified isopropanol in a 1:9 ratio (1 part of 1 M HCl and 9 parts of isopropanol). Absorbance was measured at 550 nm and a reference wavelength of 690 nm on a Multiskan Ascent[®] spectrophotometer (Labsystems, Helsinki, Finland). Cell viability was calculated using the formula: $(\text{absorbance of sample} - \text{absorbance of medium} / \text{absorbance of control} - \text{absorbance of medium}) \times 100$ for $n=4$ experiments. The IC_{50} s were then graphically obtained after generating a dose response curve using Graphpad Prism[®] software (California, USA).

2.6 Impedance measurement using the xCELLigence system

The MTT assay developed by Mosmann in 1983, (Mosmann 1983) is an endpoint assay widely used for the quantitative assessment of cellular viability and proliferation. Unfortunately because of limitations such as poor linearity with changing cell number, sensitivity to environmental conditions and the fact that it depends on only one parameter, which is the cells' metabolism of formazan (Boyd 1989; Haselsberger et al, 1996; Denizot and Lang 1986), there is the need to use additional confirmatory methods to conclude on cell status. Measuring several parameters in the same assay using dynamic conditions like the impedance technology has been shown to provide better insight on cell response patterns. Impedance

measurements were performed on the TZM-bl cells using the RT-CES™ xCELLigence system (ACEA Biosciences Inc., San Diego, USA) and following the manufacturer's instructions. This technique enables the measurement of cell response patterns in real time (providing results not possible in end point assays) and resulting in multivariate data from a single experiment. In addition, because it is label free, further downstream analysis of the same cells can be performed. The RT-CES™ system has previously been described (Solly et al, 2004; Atienza et al, 2005). The system that was used in this study is known as the dual plate (DP) and employs 3x16 well electronic plates (E-plates). The E-plate contains integral sensor electrode arrays that allows impedance measurement read out as cell index (CI) resulting from the interaction of attaching cells with the electrodes (Xing et al, 2006). This provides information on the viability or cytotoxicity as CI increases or decreases respectively. Pre-determined assay parameters such as cell culture conditions, cell number (2×10^5 cells/mL) and media volume were used. After plating the cells, the E-plates were left at room temperature for 30 min so as to reduce variability resulting from edge effects (Lundholt et al, 2003) before being transferred to the RT-CES™ analyser. After approximately 22 - 24 h of allowing the cells to attach and attain confluency of between 60-70%, the test compounds were added to the wells to final concentrations of 5, 10 and 20 μ M (250 μ L final volume). The dynamic monitoring of cell response patterns, depicting death and recovery, was automatically recorded every minute (short term) for 1 h and then every 30 min (long term) for a further 48 - 72 h. Short term monitoring allows for the identification of immediate and transient compound effects while long term monitoring enables sufficient time for the compounds to interact with the cells and modulate their targets, enabling distinctions in cell response patterns (Abassi et al, 2012). Certain compounds can immediately result in cell death (drop in CI) with the possibility of recovery (increase CI) while others are taken up at varying degrees depicted by an increase in CI over a given time period prior to a decrease. These differences in uptake, recovery and or toxicity levels could also be related to the lipophilicity of the particular compound. A normalised CI (NCI) was used to compare the effect of the compounds on the cells where impedance is set at 1 and at the time point where the cells were treated with compounds (22-24 h post seeding). When normalisation is set, it corrects for any small differences that might have occurred between cells before the addition of compounds such that only compound effects are visible.

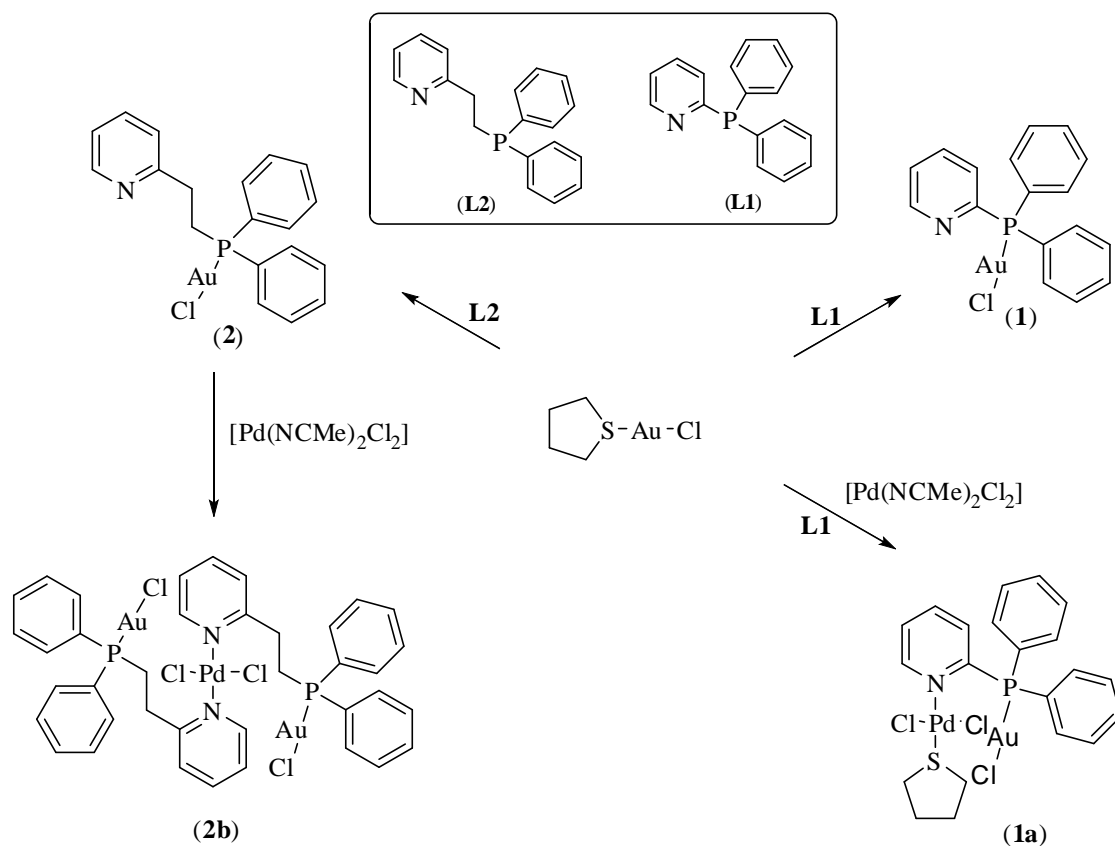
2.7 ADMET predictions to determine lipophilicity

ADMET predictions were performed using DS®, as previously described for some gold(III) thiosemicarbazonate complexes (Fonteh et al, 2011). The molecular structure of the compounds in the structural data file (sdf) format were geometrically optimised and subjected to an ADMET run. The protocol consists of various models that enable prediction of human intestinal absorption (HIA), aqueous solubility, blood brain barrier penetration (BBB), cytochrome P450 (CYP) inhibition, hepatotoxicity and plasma protein binding (PPB). It also predicts lipophilicity levels in the form of atom-based LogP (AlogP98). We have previously shown a similarity between these *in silico* lipophilicity predictions and those obtained from the wet lab shake flask method for two gold-based compounds (Fonteh et al, 2011). Considering that lipophilicity provides information on other drug-like properties such as lipid solubility, tissue distribution, receptor binding, cellular uptake, metabolism and bioavailability (Ghose et al, 1998), our main focus here was to compare the lipophilicity outcome from the ADMET predictions to the uptake profile from the real time studies. The anticipation was that the predicted lipophilicity values will correlate with the uptake, cell response and recovery patterns from the impedance study.

3 Results and Discussion

3.1 Synthesis and characterization of the complexes

Compounds **1** (Alcock et al, 1982) and **2** (Calhorda et al, 2010) have previously been synthesised but in this study both compounds were done by a slightly modified method that led to better yields; whilst compound **1a** which was prepared by adopting a one-pot approach is novel. All complexes were synthesized in good to excellent yields. The procedure outlined in Scheme 1 represents a general route for synthesis of gold(I) complexes **1**, **2** and bimetallic complex **1a**. The complexes were characterized by NMR spectroscopy and elemental analysis as well as X-ray diffraction studies for complexes **1a** and **2**.



Scheme 1: Preparation of complexes

The molecular structure of **2** (Fig S1) which was confirmed by single crystal X-ray diffraction is presented in the online resource section. The complex crystallized with one molecule in the asymmetric unit. Crystal data collection and refinement parameters are given in Table SI (online resource section) and a selection of bond lengths and angles are listed in Table SII. The coordination around the gold center deviates by about 2.7° from a perfect linear geometry. The bond angle P-Au-Cl deviates from linearity like (triphenylphosphine)gold(I) chloride complex which is $179.63(8)^\circ$. P-Au distance is within expected values while the Au-Cl distance is slightly longer than the distance for (triphenylphosphine)gold(I) chloride $2.235(3)$ Å (Baenziger et al, 1976).

A novel bimetallic complex, **1a**, was synthesized by the reaction of **L1** with [Au(THT)Cl] and [PdCl₂(NCMe)₂] in a one-pot reaction with equimolar quantities of all three reagents (Scheme 1). Complex **1a** was isolated in a very good yield. The ¹H NMR spectrum of **1a** similarly showed the characteristic phenyl resonances found in **1**. In addition to pyridine ring resonances that were observed as a doublet at 9.39 ppm corresponding to the proton *ortho* to the pyridine ring that had been shifted

downfield due to coordination, and a triplet at 7.79 ppm, a quartet at 7.67 ppm and another triplet at 7.35 ppm. The tetrahydrothiophene (THT) protons appeared as broad singlets at 3.61 ppm, 2.77 ppm, 2.31 ppm and 1.94 ppm. The $^{31}\text{P}\{^1\text{H}\}$ NMR spectrum of the monometallic gold(I) complex showed one resonance at 32.21 ppm, however, the $^{31}\text{P}\{^1\text{H}\}$ NMR spectrum of complex **1a** showed single resonance at 37.56 ppm which confirmed further coordination to palladium. The $^{13}\text{C}\{^1\text{H}\}$ NMR spectrum of dichlorobis-(tetrahydrothiophene)-palladium(II) has a doublet at 29.9 ppm and a singlet at 42.1 ppm whilst for **1a** these carbons resonated as two doublets at 29.54 and 37.7 ppm. This was further evidence that compound **1a** had a phosphine ligand, as the two doublets in the ^{13}C spectrum are the result of ^{31}P coupling with ^{13}C . The molecular structure of **1a** was confirmed using single crystal X-ray diffraction as shown in Fig 1. Crystal data collection and refinement parameters are given in Table SI, and selected bond lengths and angles for **1a** are listed in Table I and for **2** in Table SII. The geometry of **1a** has a nitrogen atom of the pyridine ring, two chlorine atoms as well as the sulfur atom of THT bound to the palladium in a four coordinate geometry. The reaction of $[\text{Au}(\text{THT})\text{Cl}]$ with **L1** leads directly to **1**. The bounded THT is indicative of a re-arrangement that led to the final product. In fact, the released THT moiety that is present in the reaction mixture filled the fourth coordination site in **1a** by coordinating to palladium through the sulphur atom. The geometry around the gold center in **1a** deviates from linearity, with a bond angle P1-Au1-Cl13 ($170.09(2)^\circ$) which deviates from linearity much more than the corresponding angle in (triphenylphosphine)gold(I) chloride ($179.63(8)^\circ$) reported in the literature (Baenziger et al, 1976). The gold-phosphorous distance P1-Au1 ($2.199(10)$ Å) is however slightly shorter than the distance for (triphenylphosphine)gold(I) chloride ($2.235(3)$ Å). The geometry around the Pd atom in the complex is a distorted square planar geometry with N1-Pd1-Cl11 ($88.13(6)^\circ$), N1-Pd1-Cl12 ($90.71(6)^\circ$), S1-Pd1-Cl11 ($87.37(4)^\circ$), and S1-Pd1-Cl12 ($92.87(4)^\circ$). For *trans*-dichlorobis(tetrahydrothiophene)palladium(II) the similar angles for S1-Pd1-Cl11 and S1-Pd1-Cl12 are $84.33(5)^\circ$ and $95.67(5)^\circ$ respectively (Norén et al, 1997). The N1-Pd1 ($2.058(2)$ Å), Pd1-Cl11 ($2.2976(90)$ Å) and Pd1-Cl12 ($2.3054(9)$ Å) bond distances are shorter than the corresponding distances for $[\text{Pd}(\text{CH}_3)\text{Cl}(\text{C}_{26}\text{H}_{24}\text{NP})]$ (Agostinho et al, 2006). The solvent chloroform has the expected structure, with bond lengths Cl4-C22 = $1.747(3)$ Å, Cl5-C22 = $1.767(3)$ Å, and Cl6-C22 = $1.762(3)$ Å.

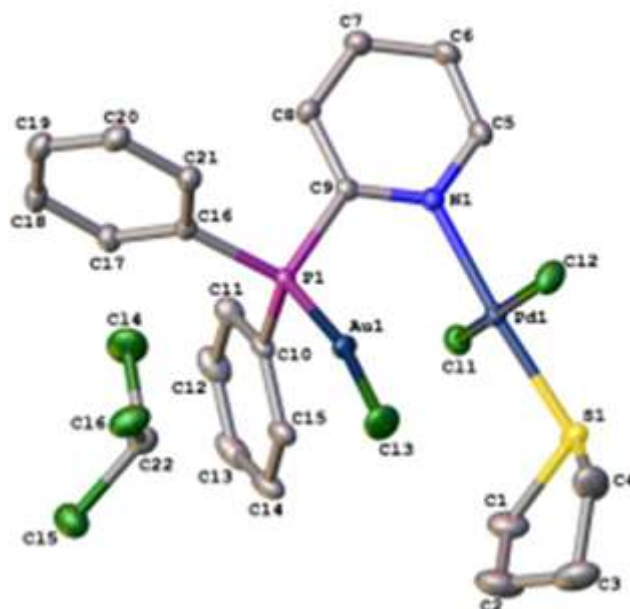


Fig 1: Molecular structure of **1a** with 50% probability ellipsoids. The ORTEP diagram is presented for the purpose of showing the connectivity of the atoms. Hydrogen atoms are omitted for clarity.

Table I: Selected bond distances (Å) and angles (°) for **1a**. The numbers in parenthesis are estimated standard deviations.

Bond length (Å)		Bond angles (°)	
Au1-P1	2.2199(0.0001)	P1-Au1-Cl3	170.09(2)
Au1-Cl3	2.2907(0.0001)	N1-Pd1-Cl1	88.13(6)
Pd-N1	2.058(2)	N1-Pd-Cl2	90.71(6)
		S1-Pd1-Cl2	87.37(4)

An attempt to synthesise a second bimetallic complex (**2a**) with formula $\text{AuPd}(\mathbf{L2})(\text{SC}_4\text{H}_8)\text{Cl}_3$, from **L2** in order to investigate the structure activity relationship (SAR) with **1**, **1a** and **2** was initiated. Unfortunately **2a** was found to be unstable and was only considered for the *in silico* ADMET predictions and not for the bioassays. The reason for this is because the *in silico* findings depend on computer aided structure predictions only and can potentially provide some predictive information on **2a**'s effect on cells thereby enabling comparison with those of **1**, **1a** and **2**.

Further investigation by NMR and X-ray spectroscopy of the reaction mixture of the supposed instable second bimetal (**2a**) confirmed the presence of traces of **2b**, $\text{Au}_2\text{Pd}(\mathbf{L2})_2\text{Cl}_4$, in solution (Scheme 1), also previously synthesised by Calhorda *et al.* (Calhorda et al, 2010), hence no spectral data is presented. This complex unlike **1a** and the proposed **2a** structure is structurally bulkier containing two Au atoms, each independently linked to **L2** and bridged by a Pd atom coordinated to the nitrogen atom of the pyridine ring

of both **L2** moieties. Interestingly, the impedance data and ADMET predictions for **2b** were not comparable to that of **1a** probably because of these significant structural differences and as such are only briefly discussed.

3.2 MTT assay for toxicity determination

In the MTT study, dose dependent increases in toxicity were observed for the complexes and not the ligands (Fig 2). At the tested concentrations, ligands **L1** and **L2** had no adverse effects on the viability of the cells ($IC_{50} > 100 \mu M$). IC_{50} values for the metal complexes were much lower suggesting increased toxicity resulting from complexation of the ligands with metals. These were $12.5 \pm 2.5 \mu M$, $18.3 \pm 8.3 \mu M$, and $16.9 \pm 0.5 \mu M$ for complexes **1**, **1a** and **2** respectively. A notable observation was the fact that **1** was more toxic than **2**. The presence of the ethyl group in **L2** and thus **2** which is absent in **1** (**L1**) might play a role in the reduced toxicity of the former. Although the monometallic complex appeared slightly more toxic than the bimetallic complex e.g. complex **1** with an IC_{50} of $12.5 \pm 2.5 \mu M$ compared to **1a** with IC_{50} of $18.3 \pm 8.3 \mu M$, the higher deviation from the mean as seen in the standard error of the means for the bimetallic complex over the monometallic ones appeared to cancel this out. This high deviation for the bimetal could be attributable to the structural differences such as the presence of the dichloro(tetrahydrothiophene)palladium(II) moiety and hence differences in drug-like properties such as lipophilicity, uptake and hence metabolism. The lipophilicity outcome and cytotoxicity correlation are further discussed in the real time and the *in silico* ADMET prediction studies to further clarify this difference.

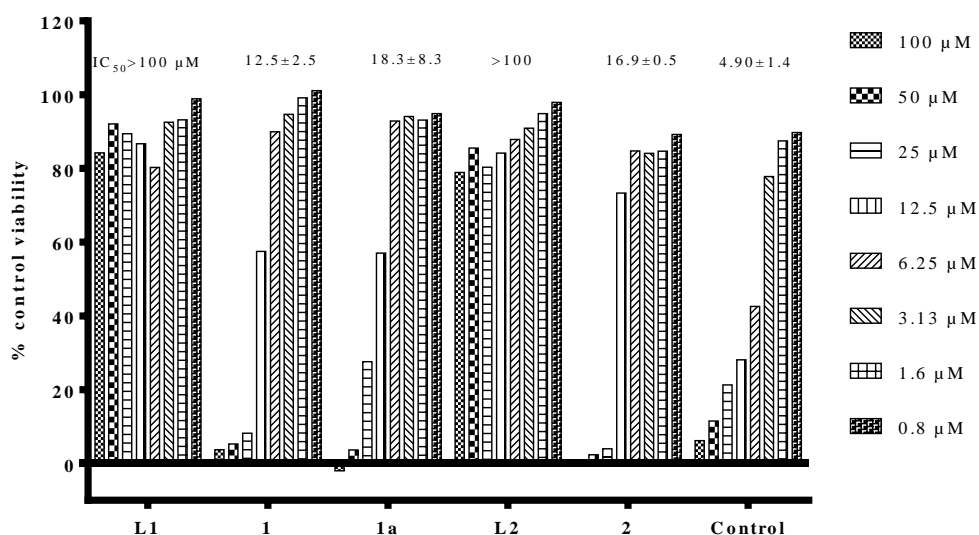


Fig 2: Effect of compounds on the viability of TZM-bl cells analysed using the MTT tetrazolium dye. Two fold serially diluted concentrations from 100 to 0.8 μM were tested and a dose dependent decrease in viability was observed for the mono- and bi-metallic compounds. IC_{50} values obtained were $>100 \mu\text{M}$ for **L1** and **L2** and $12.5 \pm 2.5 \mu\text{M}$, $18.3 \pm 8.3 \mu\text{M}$ and $16.9 \pm 0.5 \mu\text{M}$ for complexes **1**, **1a**, and **2** respectively. The monometallic compounds, **1** and **2** were more toxic than bimetallic compound, **1a**. A 10 μM the IC_{50} value of auranofin which was used as control was $4.9 \pm 1.4 \mu\text{M}$. The IC_{50} was calculated from four independent experiments performed in triplicate.

3.3 RT-CESTM findings show distinguishing uptake and recovery patterns between mono- and bi-metallic compounds.

Results for the impedance profiles of the complementary metallic complexes (**1** and **1a**) of **L1** are shown in Fig 3. Three concentrations of 5, 10 and 20 μM were tested and only one concentration of 10 μM for **L1** (insert Fig 3). A dose dependent decrease in CI was observed from 5 to 20 μM , representative of increasing cell death or decreasing cell proliferation when the TZM-bl cells were treated with the metal complexes. At 10 μM , the effect of **L1** did not result in CI decreases supporting the MTT findings where the IC_{50} was reported to be $> 100 \mu\text{M}$ (insert Fig 3). This finding also supports the fact that the activity/toxicity of the metal complex is as a result of the presence of the metal entity (Navarro 2009; Beraldo and Gambino 2004) which in addition to structurally stabilising the organic moiety or ligand (Navarro 2009), also improves activity.

Following complex addition, there was an observed steady increase in CI which peaked by 1 h for **1** and 2nd hour for **1a** compared to the untreated cells. This peaking in CI has been associated with compound uptake due to swelling (Thakur et al, 2012) or to result from cell fusion forming multinuclear bodies

(Xing et al, 2005). Four independent Sybergreen staining assays, detected using flow cytometry to determine multinuclear body formation indicated that only 1N nuclei and not 2N were present (data not shown). The resultant increase in CI shortly after the addition of **1** and **1a** was thus more likely as a result of uptake and swelling of the cells and not multinuclear fusion. This uptake was expected since lipophilic metal complexes are known to enter cells by passive diffusion across the membrane potential (Puckett et al, 2010). The variation in uptake time (peak area) prior to the time point when a sustained decrease in CI (below cell control) was observed was used in comparing the lipophilicity and hence uptake profiles of the phosphine metal complexes in this study. At the more toxic 20 μ M concentration (also $>IC_{50}$), the uptake time (and subsequent cell death) for cells treated with **1** was shorter than for cells treated with **1a** suggesting that more of **1a** accumulated in the cells and not **1** (Fig 4a). The area under this peak for three independent experiments was found to be 0.2 ± 0.2 and 1.3 ± 0.4 for **1** and **1a** respectively, further supporting this observation.

At the non toxic 10 μ M ($<IC_{50}$), no significant differences in the uptake pattern of the complexes were observed compared to untreated cells (Fig 4a). Instead, recovery patterns, where near constant cell indices (CIs) started increasing with time, were observed. These observations were more noticeable and occurred earlier for **1a** than for **1** (Fig 4a) further supporting the MTT end point findings where **1a** was shown to be less toxic than **1**. CI decreases caused by **1** took much longer to reach a near constant point (10h 30 min post treatment or PT) and longer (40 h 30 min PT) to reach recovery point compared to **1a** for which there was a brief or absent near constant point due to a quicker recovery time starting 10 h 30 min PT (Fig 4a). In an end point assay such as MTT, it would be difficult to determine cell recovery rate and time and thus determine which compound resulted in quicker recovery over the other since the staining process does not allow for real time monitoring (Xing et al, 2006).

The real time studies were performed at least three times for **1** and **1a** at 5, 10 and 20 μ M and at these concentrations, similar uptake and recovery patterns were obtained. The data shown in Fig 3 is a representative of the three while two additional profiles are shown in Fig S2 of the online resource data. This data further confirms the relatedness between uptake, recovery, lipophilicity and structure. The main differences in proliferation patterns and toxicity of **1** and **1a** could be attributed to the presence of the dichloro(tetrahydrothiophene)palladium(II) moiety present in **1a** which is absent in **1**. The uptake patterns

seen for the bimetal **1a**, where there was a significant increase in CI upon compound addition has previously been shown for a bimetallic gold(I) phosphine complex designated EK207 (Fonteh 2011).

In the impedance studies, a dose dependent decrease in CI was also observed for **2** at 5, 10 and 20 μM (depicted in Fig S3). At 10 μM recovery was slower, findings that were similar to those of **1** (Fig S4). When the proliferation patterns of **1** and **2** were compared (Fig S4), it was evident that recovery for **2** was better than for **1**. This again may be linked to the presence of the ethyl group and supports the MTT findings where **1** was more toxic than **2** (IC_{50} 12.5 ± 2.5 and 16.9 ± 0.5 μM respectively)..

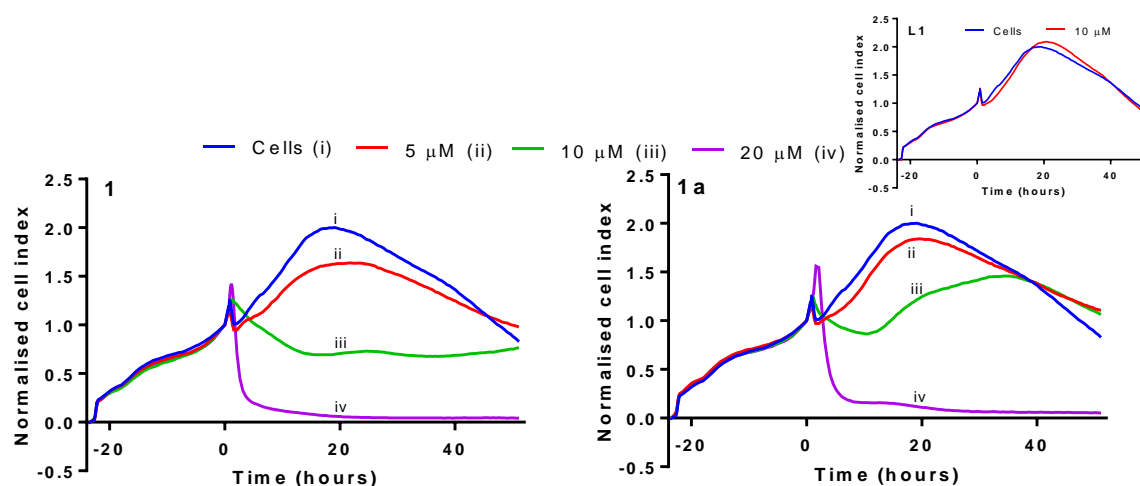
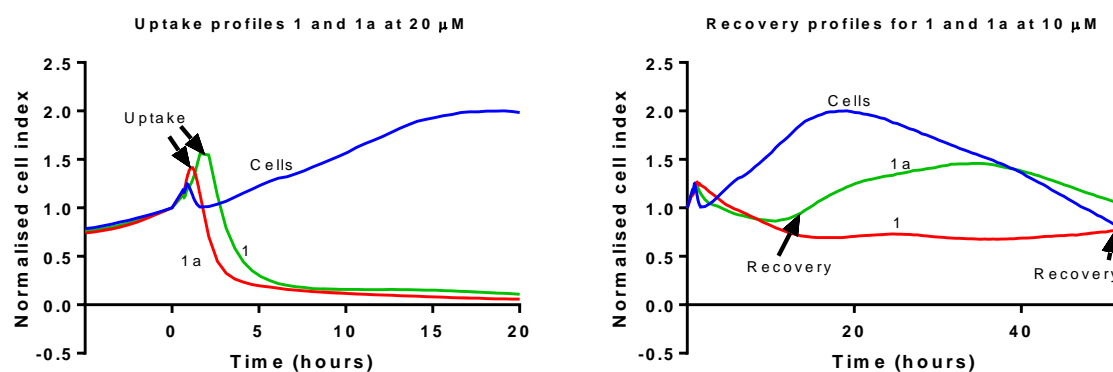


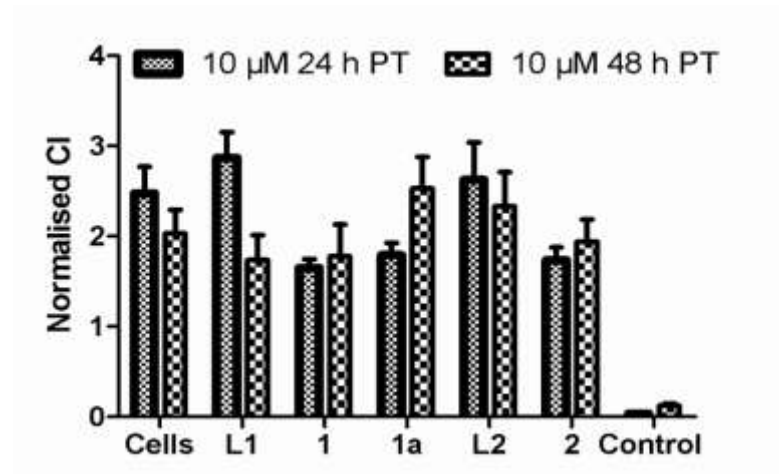
Fig 3: Effect of the Au monometallic complex **1** and the Au-Pd bimetallic complex **1a** on the impedance profile of TZM-bl cells. TZM-bl cells were plated and allowed to adhere for 23.30 h before treatment with 5, 10 and 20 μM of **1** and **1a**. Normalisation was done 23.30 h. Dose dependent changes in CI were observed for **1** and **1a** at the tested concentrations with **1** being more toxic than **1a**.

To further compare uptake and recovery patterns between the monometallic and bimetallic complexes, a cumulative time point plot of the CIs at 24 h and 48 h PT and at 10 μM only were compared (Fig 4b). The average of at least three different repeats were analysed. At these two time points, the CI for the monometallic compounds (**1** and **2**) were lower than those of the bimetallic complex (**1a**) especially at 48 h, further supporting the toxicity and recovery trends observed in the real time and MTT study. Over time (from 24 to 48 h PT), CI was seen to decrease for **L1** and **L2** and the untreated control (probably due to overcrowding and hence cell death) while an increase was observed for the complexes as a result of recovery. Based on this time study, the gold complexes appeared slightly more toxic after 24 h but not after 48 h (when recovery was occurring), findings which will otherwise not be noticeable in the end point

MTT assay. For the complexes, the CIs were always higher for the bimetallic than for the monometallic complexes further correlating the fact that the former were less toxic compared to the latter.



A



B

Fig 4: Comparative uptake and recovery profiles between the mono and bimetallic complexes. A comparison of uptake of **1** with that of **1a** at 20 μM showed that **1** was taken up more rapidly than **1a** (Fig 4a). As a result, recovery of cells treated with **1** at 10 μM was slower than for **1a** (Fig 4a). A quantitative representation of complex mediated effect post treatment is shown in Fig 4b. CI increases were observed for **L1**, **L2** and the untreated control at 24 h post treatment depicting cell viability but at 48 h PT, decreases were observed probably as a result of overcrowding and hence cell death. For the complexes, the reverse was observed with CI decreases 24 h PT and increases at 48 h PT which is associated with the observed recovery. PT stands for post treatment. Recovery was better for the bimetallic complex over the monometallic ones. At 10 μM, auranofin which was used as control for cell death resulted in CI values both similar to those obtained for the media control confirming ~100% cell death.

3.4 ADMET Predictions to determine lipophilicity

The importance of determining drug-likeness in the early stages of drug discovery has resulted in the development of numerous prediction tools. These tools enable the sorting of new drug candidates early on in the discovery process such that more safe drugs get into the more costly, late drug developmental phases (Donato et al, 2008). The use of the rule of five which states that poor absorption or permeation is more likely when there are > 5 H-bond donors, >10 H-bond acceptors, the molecular weight (Mr) is > 500 and when the calculated log P is > 5 (Lipinski et al, 1997) is an example of one such prediction method. Here we have employed the ADMET protocol in DS® which aids in the prediction of aqueous solubility, BBB penetration, CYP inhibition, hepatotoxicity, HIA and PPB. AlogP98 and polar surface area (PSA, related to the H-bonding ability) are also some of the predicted parameters. To enable comparison of the lipophilicity profile of the monometallic and bimetallic complexes, predictions were also done for **2a**. The instability reported for **2a** in the wet lab synthesis was not a concern here since this is an *in silico* computer aided study and does not require the synthetic product.

For the purposes of this study, the predicted lipophilicity values (AlogP98) will be the main focus of the discussion since lipophilicity provides information on other drug-like properties such as lipid solubility, tissue distribution, receptor binding, cellular uptake, metabolism and bioavailability (Ghose et al, 1998). The lipophilicity levels were compared to the xCELLigence profiles to determine if there was correlation in uptake and recovery patterns. These will be further discussed with respect to aqueous solubility and HIA. The predicted HIA, aqueous solubility and lipophilicity values are shown in Table II. Ligands **L1** and **L2** and the monometallic complexes **1** and **2** were predicted as having ideal lipophilicity (AlogP98≤5), HIA and aqueous solubility based on the rankings that were returned unlike the bimetallic ones, **1a** and **2a** respectively (Table II).

Four prediction levels (0-4) are provided to aid in the classification of HIA. A classification of zero indicates good HIA while 4 is very poor absorption. The ligands and monometallic compounds were all predicted as having an HIA of 0 (good) while the bimetallic compounds resulted in an HIA level of 2 (low). With regards to aqueous solubility, six levels are described were 0 is extremely low, 1 very low but possible, 2 is low, 3 good, 4 optimal, 5 too soluble and 6 a warning suggesting that molecules with one or more unknown AlogP98 types are present. Ligands **L1**, **L2**, and monometallic complexes, **1** and **2** were again predicted to have a ranking of 2 (low) unlike bimetallic ones **1a** and **2a** with a prediction of 1 (very

Table II: ADMET prediction scores for the compounds. These scores were predicted using DSTM (Accelrys, California, USA). Various rankings come with the protocol. For **L1**, **L2**, **1** and **2**, a ranking of 0 represented good HIA while 2 for bimetallic compounds, **1a** and **2a** suggested a low HIA. Aqueous solubility level of 2 is classified as low for **L1**, **L2**, **1** and **2** while **1a** and **2a** were classified as possible (1). An AlogP98 or lipophilicity >5 is poor and was shown for **1a** and **2a** and ≤5 is ideal lipophilicity as was the case for **L1**, **L2**, **1** and **2**. Unknown AlogP98 are the number of atoms in the compound with unknown AlogP98 which is common for the metal complexes and not the ligands.

	L1	1	1a	L2	2	2a	Auranofin
HIA	0	0	2	0	0	2	0
Aqueous Solubility level	2	2	1	2	2	1	4
Alogp98	4.56	4.91	6.55	5.03	4.84	6.48	1.41

low but possible). With regards to lipophilicity, the Lipinski's rule of 5 (Lipinski et al, 1997) was used as a guide to classify predictions where compounds with lipophilicity of >5 were considered to have poor absorption and permeation. Based on this classification, the bimetallic complexes again were the least drug-like with AlogP98 values of 6.55 and 6.48 for **1a** and **2a** respectively while the ligands and monometallic complexes were all predicted as having AlogP98 values of 5 and below (Table II).

The bimetallic complexes which were less toxic in the MTT study (Fig 2) were predicted to have non ideal lipophilicity values (> 5) according to Lipinski *et al.*, (Lipinski et al, 1997), limited aqueous solubility and HIA levels and thus poor absorption. Generally, compounds with ideal lipophilicity values, like the case of **L1**, **L2**, **1** and **2**, demonstrate good aqueous solubility and are usually taken up better compared to poorly soluble compounds. The presence of the ethyl moiety in **2** and not **1** appeared to also influence lipophilicity (4.91 and 4.84 respectively) and to minimally affect uptake and recovery compared to **1a** (Fig S4). This was also observed in the slight differences seen in toxicity patterns (IC₅₀ of 12.5±2.5 for **1** and 16.9±0.5 μM for **2**).

Considering that lipophilicity predictions and thus HIA and aqueous solubility were limiting for **1a** and **2a**, it is not surprising that uptake of **1a** (a bimetal) at the toxic concentration of 20 μM occurred at a slower pace (peak area of 1.3±0.4 compared to 0.2 ±0.17 for **1**) such that recovery was quicker at 10 μM (Fig 4a). The poor aqueous solubility as a result of high lipophilicity also meant more of the free compound was available in solution. If this was the case, the likelihood of the free compound interfering with MTT metabolism was higher and might be the reason for the high standard error of means observed in the MTT assay for **1a**. Such a limitation will be obviated in the xCELLigence assay considering the label-free nature. It was therefore exciting to note that despite the possible MTT limitation, there was correlation between the two studies.

The lipophilicity prediction value of 1.41 for auranofin (Table II), which was used as a control in this study, supports literature reports where the latter compound has been orally used as an anti-arthritic gold-based compound because of its ideal lipophilicity (Shapiro and Masci 1996).

Toxicity, impedance and ADMET findings for complex **2b** (product obtained when **2a** synthesis was attempted) are shown in Table SIII. The complex was slightly more toxic as seen from both the IC₅₀ and impedance profile. The predicted AlogP98 was 10.66 indicative of poor HIA and aqueous solubility (Table SIII). This compound which has two gold atoms and lacks the THT moiety present in **1a** presented a profile which was not supportive of the SAR. This finding was not surprising but suggests that using impedance for drug-likeness correlation should only serve to complement other techniques since different ligands or moieties which coordinate to metals differently could alter ADMET properties significantly.

4. CONCLUSION

Testing new chemical entities for cytotoxicity and drug-likeness are common in the very early stages of a drug discovery project so as to limit failure later in the more costly phases. Rational drug design has been instrumental in this process but the focus has also been on designing libraries based on biological principles (McGuinness 2007). Metal compounds such as gold and palladium have been studied for anticancer activity and for their effects on a wide range of microorganisms making them candidate compounds in drug discovery as either in the mono or bimetallic forms. While it has been reported that varying the lipophilicity and hydrophilicity of some gold-based compounds results in better selectivity and hence reduced toxicity (Berners-Price et al, 1999) due to the correlation in uptake (McKeage et al, 2000), to the best of our knowledge, using impedance technology to monitor these correlations and how it is altered in the presence of a second metal or group to show SAR has not been reported.

In this study, the drug-likeness of two monometallic gold-based compounds (**1** and **2**) and a bimetallic Au-Pd complex (**1a**) were investigated using an end point cytotoxicity assay, a real time impedance assay (which produces multivariate data) and lipophilicity predictions were done using an *in silico* technique. The monometallic complexes were slightly more toxic than the bimetal as depicted by IC₅₀ values but presented ideal lipophilicity, aqueous solubility and hence better cellular uptake. Overall, these qualities classify the bimetallic complex as a poor drug candidate since compounds with limited uptake will generally not reach cellular targets (thus not orally available) but will cause irreversible cell membrane

damage especially at high concentrations. Although the findings appear to be applicable to compounds with minimal diversity in structure, the multivariate information obtained from the RT-CES study could be useful in the filtering out these types of compounds to identify the most drug-like for further biological testing.

5. ONLINE RESOURCE MATERIAL

An online resource section is included as a separate document

Appendix A. online resource data

CCDC numbers <884806> and <960995> contains the online resource crystallographic data for **2** and **1a**, respectively. These data can be obtained free of charge via <http://www.ccdc.cam.ac.uk/conts/retrieving.html>, or from the Cambridge Crystallographic Data Centre, 12 Union Road, Cambridge CB2 1EZ, UK; fax: (+44) 1223-336-033; or e-mail: deposit@ccdc.cam.ac.uk.

6. LIST OF IMPORTANT ABBREVIATIONS

ADMET: absorption, distribution, metabolism, excretion, toxicity

AlogP98: atom based log P

BBB: blood brain barrier

IC₅₀: 50% inhibitory concentration

CI: cell index

CI_s: cell indices

CYP: cytochrome P450

DS: Discovery Studio

HIA: human intestinal absorption

HIV: human immunodeficiency virus

MTT: 3-(4,5-dimethylthiazol-2-yl)-2,5-diphenyltetrazolium bromide

NCI: normalised cell index

PPB: plasma protein binding

PT: post treatment

RT-CES: real time cell electronic sensing.

SAR: structure activity relationship

7. ACKNOWLEDGEMENTS

The authors would like to thank the Technology Innovation Agency (TIA) and the University of Pretoria for financial support. A. Elkhadir is grateful to the Organization for Women in Science for the Developing World (OWSD) formerly Third World Organization for Women in Science (TWOWS) and University of Johannesburg for financial support.

8. CONFLICT OF INTERESTS

The authors declare that they have no competing interests.

9. REFERENCES

Abassi YA, Xi B, Li N, Ouyang W, Seiler A, Watzele M, Kettenhofen R, Bohlen H, Ehlich A, Kolossov E, Wang X, Xu X, (2012) Dynamic monitoring of beating periodicity of stem cell-derived cardiomyocytes as a predictive tool for preclinical safety assessment. *Br.J.Pharmacol.* 165: 1424-1441. doi: 10.1111/j.1476-5381.2011.01623.x; 10.1111/j.1476-5381.2011.01623.x.

Agostinho M, Banu A, Braunstein P, Welter R, Morise X, (2006) New palladium complexes with phosphino- and phosphinitopyridine ligands. *Acta Crystallogr.C* 62: m81-6. doi: 10.1107/S0108270106001296.

Alcock NW, Moore P, Lampe PA, Mok K, (1982) Crystal and molecular structures of two complexes of diphenyl (2-pyridyl) phosphine (L):[AuClL] and [Ag₂Cl₂L₃]. *J.Chem.Soc., Dalton Trans.* 207-210.

Altomare A, Cascarano G, Giacovazzo C, Guagliardi A, (1993) Completion and refinement of crystal structures with SIR92. *Journal of Applied Crystallography* 26: 343-350.

Atienza JM, Zhu J, Wang X, Xu X, Abassi Y, (2005) Dynamic monitoring of cell adhesion and spreading on microelectronic sensor arrays. *Journal of biomolecular screening* 10: 795-805.

Baenziger N, Bennett W, Soborofe D, (1976) Chloro (triphenylphosphine) gold (I). *Acta Crystallographica Section B: Structural Crystallography and Crystal Chemistry* 32: 962-963.

Beraldo H, Gambino D, (2004) The wide pharmacological versatility of semicarbazones, thiosemicarbazones and their metal complexes. *Mini Rev.Med.Chem.* 4: 31-39.

Berners-Price SJ, Bowen RJ, Galettis P, Healy PC, McKeage MJ, (1999) Structural and solution chemistry of gold (I) and silver (I) complexes of bidentate pyridyl phosphines: Selective antitumour agents. *Coord.Chem.Rev.* 185: 823-836.

Boyd MR, (1989) Status of the NCI preclinical antitumor drug discovery screen. *Cancer: Principles and Practice of Oncology Updates* 3: 1-12.

- Boyd JM, Huang L, Xie L, Moe B, Gabos S, Li XF, (2008) A cell-microelectronic sensing technique for profiling cytotoxicity of chemicals. *Anal.Chim.Acta* 615: 80-87. doi: 10.1016/j.aca.2008.03.047.
- Bruker A, (2009) APEX2—software suite for crystallographic programs. Bruker AXS Inc., Madison .
- Calhorda MJ, Ceamanos C, Crespo O, Gimeno MC, Laguna A, Larraz C, Vaz PD, Villacampa MD, (2010) Heteropolynuclear gold complexes with metallophilic interactions: Modulation of the luminescent properties. *Inorg.Chem.* 49: 8255-8269.
- Denizot F, Lang R, (1986) Rapid colorimetric assay for cell growth and survival. modifications to the tetrazolium dye procedure giving improved sensitivity and reliability. *J.Immunol.Methods* 89: 271-277.
- Derdeyn CA, Decker JM, Sfakianos JN, Wu X, O'Brien WA, Ratner L, Kappes JC, Shaw GM, Hunter E, (2000) Sensitivity of human immunodeficiency virus type 1 to the fusion inhibitor T-20 is modulated by coreceptor specificity defined by the V3 loop of gp120. *J.Virol.* 74: 8358-8367.
- Donato MT, Lahoz A, Castell JV, Gomez-Lechon MJ, (2008) Cell lines: A tool for in vitro drug metabolism studies. *Curr.Drug Metab.* 9: 1-11.
- Farrugia LJ, (1999) WinGX suite for small-molecule single-crystal crystallography. *Journal of Applied Crystallography* 32: 837-838.
- Farrugia LJ, (1997) ORTEP-3 for windows-a version of ORTEP-III with a graphical user interface (GUI). *Journal of Applied Crystallography* 30: 565-565.
- Fonteh PN, (2011) Gold Compounds with Anti-HIV and Immunomodulatory Activity .
- Fonteh PN, Keter FK, Meyer D, (2011) New bis(thiosemicarbazone) gold(III) complexes inhibit HIV replication at cytostatic concentrations: Potential for incorporation into virostatic cocktails. *J.Inorg.Biochem.* 105: 1173-1180. doi: 10.1016/j.jinorgbio.2011.05.011; 10.1016/j.jinorgbio.2011.05.011.
- Fonteh PN, Keter FK, Meyer D, Guzei IA, Darkwa J, (2009) Tetra-chloro-(bis-(3,5-dimethylpyrazolyl)methane)gold(III) chloride: An HIV-1 reverse transcriptase and protease inhibitor. *J.Inorg.Biochem.* 103: 190-194. doi: 10.1016/j.jinorgbio.2008.10.001.
- Ghose AK, Viswanadhan VN, Wendoloski JJ, (1998) Prediction of hydrophobic (lipophilic) properties of small organic molecules using fragmental methods: An analysis of ALOGP and CLOGP methods. *The Journal of Physical Chemistry A* 102: 3762-3772.
- Giaever I, Keese CR, (1984) Monitoring fibroblast behavior in tissue culture with an applied electric field. *Proceedings of the National Academy of Sciences* 81: 3761-3764.
- Hamid R, Rotshteyn Y, Rabadi L, Parikh R, Bullock P, (2004) Comparison of alamar blue and MTT assays for high through-put screening. *Toxicol.In.Vitro.* 18: 703-710. doi: 10.1016/j.tiv.2004.03.012.
- Haselsberger K, Peterson DC, Thomas DG, Darling JL, (1996) Assay of anticancer drugs in tissue culture: Comparison of a tetrazolium-based assay and a protein binding dye assay in short-term cultures derived from human malignant glioma. *Anticancer Drugs* 7: 331-338.
- Kepp O, Galluzzi L, Lipinski M, Yuan J, Kroemer G, (2011) Cell death assays for drug discovery. *Nat.Rev.Drug Discov.* 10: 221-237. doi: 10.1038/nrd3373.
- Lipinski CA, Lombardo F, Dominy BW, Feeney PJ, (1997) Experimental and computational approaches to estimate solubility and permeability in drug discovery and development settings. *Adv.Drug Deliv.Rev.* 23: 3-25. doi: DOI: 10.1016/S0169-409X(96)00423-1.

- Lobell M, Sivarajah V, (2003) In silico prediction of aqueous solubility, human plasma protein binding and volume of distribution of compounds from calculated pKa and AlogP98 values. *Mol.Divers.* 7: 69-87.
- Lundholt BK, Scudder KM, Pagliaro L, (2003) A simple technique for reducing edge effect in cell-based assays. *Journal of Biomolecular Screening* 8: 566-570.
- McGuinness R, (2007) Impedance-based cellular assay technologies: Recent advances, future promise. *Current Opinion in Pharmacology* 7: 535-540. doi: <http://dx.doi.org/10.1016/j.coph.2007.08.004>.
- McKeage MJ, Berners-Price SJ, Galettis P, Bowen RJ, Brouwer W, Ding L, Zhuang L, Baguley BC, (2000) Role of lipophilicity in determining cellular uptake and antitumour activity of gold phosphine complexes. *Cancer Chemother.Pharmacol.* 46: 343-350.
- Monim-ul-Mehboob M, Altaf M, Fettouhi M, Isab AA, Wazeer MI, Shaikh MN, Altuwaijri S, (2013) Synthesis, spectroscopic characterization and anti-cancer properties of new gold (III)-alkanediamine complexes against gastric, prostate and ovarian cancer cells; crystal structure of [Au₂(pn)₂(cl)₂]·2H₂O. *Polyhedron* 61: 225-234.
- Mosmann T, (1983) Rapid colorimetric assay for cellular growth and survival: Application to proliferation and cytotoxicity assays. *J.Immunol.Methods* 65: 55-63.
- Navarro M, (2009) Gold complexes as potential anti-parasitic agents. *Coord.Chem.Rev.* 253: 1619-1626. doi: DOI: 10.1016/j.ccr.2008.12.003.
- Nobili S, Mini E, Landini I, Gabbiani C, Casini A, Messori L, (2010) Gold compounds as anticancer agents: Chemistry, cellular pharmacology, and preclinical studies. *Med.Res.Rev.* 30: 550-580.
- Norén B, Oskarsson A, Svensson C, (1997) Cis/trans influences on bond distances in square-planar complexes. crystal structure of trans-dichlorobis (tetrahydrothiophene) palladium (II) and trans-dichlorobis (tetrahydrothiophene) platinum (II). *Acta Chem.Scand.* 51: 289-294.
- Okada T, Patterson BK, Ye SQ, Gurney ME, (1993) Aurothiolates inhibit HIV-1 infectivity by gold(I) ligand exchange with a component of the virion surface. *Virology* 192: 631-642. doi: 10.1006/viro.1993.1079.
- Palatinus L, Chapuis G, (2007) SUPERFLIP-a computer program for the solution of crystal structures by charge flipping in arbitrary dimensions. *Journal of Applied Crystallography* 40: 786-790.
- Platt E, Wehrly K, Kuhmann S, Chesebro B, Kabat D, (1998) Effects of CCR5 and CD4 cell surface concentrations on infections by 820 macrophagetropic isolates of human immunodeficiency virus type 1. *J.Virol.* 821: 2855-2864.
- Puckett CA, Ernst RJ, Barton JK, (2010) Exploring the cellular accumulation of metal complexes. *Dalton Transactions* 39: 1159-1170.
- Ray S, Mohan R, Singh JK, Samantaray MK, Shaikh MM, Panda D, Ghosh P, (2007) Anticancer and antimicrobial metallopharmaceutical agents based on palladium, gold, and silver N-heterocyclic carbene complexes. *J.Am.Chem.Soc.* 129: 15042-15053.
- Rülke R, Han I, Elsevier C, Vrieze K, Van Leeuwen P, Roobeek C, Zoutberg M, Wang Y, Stam C, (1990) New neutral and cationic methylpalladium (II) complexes containing tridentate nitrogen ligands. synthesis, reactivity and x-ray crystal structure of {σ-(N-2-(N-isopropylcarbaldimino)-6-(N-isopropylcarbaldimino)-σ-N-pyridyl)}(chloro) methylpalladium (II) and [σ³-N₃N',N''-2, 2'-6', 2''-terpyridyl} methylpalladium (II)] chloride dihydrate. *Inorg.Chim.Acta* 169: 5-8.

- Rupesh K, Deepalatha S, Krishnaveni M, Venkatesan R, Jayachandran S, (2006) Synthesis, characterization and in vitro biological activity studies of Cu–M (M= Cu²⁺, Co²⁺, Ni²⁺, Mn²⁺, Zn²⁺) bimetallic complexes. *Eur.J.Med.Chem.* 41: 1494-1503.
- Shapiro DL, Masci JR, (1996) Treatment of HIV associated psoriatic arthritis with oral gold. *J.Rheumatol.* 23: 1818-1820.
- Shaw III CF, Isab AA, Hoeschele JD, Starich M, Locke J, Schulteis P, Xiao J, (1994) Oxidation of the phosphine from the auranofin analog, triisopropylphosphine (2, 3, 4, 6-tetra-O-acetyl-1-thio-β-D-glucopyranosato-S) gold (I), via a protein-bound phosphonium intermediate. *J.Am.Chem.Soc.* 116: 2254-2260.
- Sheldrick GM, (2008) A short history of SHELX. *Acta Crystallogr., A, Found.Crystallogr.* 64: 112-122.
- Solly K, Wang X, Xu X, Strulovici B, Zheng W, (2004) Application of real-time cell electronic sensing (RT-CES) technology to cell-based assays. *Assay and drug development technologies* 2: 363-372.
- Sun RW, Che C, (2009) The anti-cancer properties of gold (III) compounds with dianionic porphyrin and tetradentate ligands. *Coord.Chem.Rev.* 253: 1682-1691.
- Takeuchi Y, McClure MO, Pizzato M, (2008) Identification of gammaretroviruses constitutively released from cell lines used for human immunodeficiency virus research. *J.Virol.* 82: 12585-12588. doi: 10.1128/JVI.01726-08.
- Thakur M, Mergel K, Weng A, Frech S, Gilabert-Oriol R, Bachran D, Melzig MF, Fuchs H, (2012) Real time monitoring of the cell viability during treatment with tumor-targeted toxins and saponins using impedance measurement. *Biosensors and Bioelectronics* 35: 503-506.
- Uson R, Laguna A, Laguna M, Briggs D, Murray H, Fackler J, (1989) (Tetrahydrothiophene) gold (I) or gold (III) complexes. *Inorganic Syntheses, Volume 26* 85-91.
- Wang C, Shih W, Chang HC, Kuo Y, Hung W, Ong T, Li W, (2011) Preparation and characterization of amino-linked heterocyclic carbene palladium, gold, and silver complexes and their use as anticancer agents that act by triggering apoptotic cell death. *J.Med.Chem.* 54: 5245-5249.
- Wei X, Decker JM, Liu H, Zhang Z, Arani RB, Kilby JM, Saag MS, Wu X, Shaw GM, Kappes JC, (2002) Emergence of resistant human immunodeficiency virus type 1 in patients receiving fusion inhibitor (T-20) monotherapy. *Antimicrob.Agents Chemother.* 46: 1896-1905.
- Xing JZ, Zhu L, Gabos S, Xie L, (2006) Microelectronic cell sensor assay for detection of cytotoxicity and prediction of acute toxicity. *Toxicol.In.Vitro.* 20: 995-1004. doi: 10.1016/j.tiv.2005.12.008.
- Xing JZ, Zhu L, Jackson JA, Gabos S, Sun XJ, Wang XB, Xu X, (2005) Dynamic monitoring of cytotoxicity on microelectronic sensors. *Chem.Res.Toxicol.* 18: 154-161. doi: 10.1021/tx049721s.
- Zhang Y, Hess EV, Pryhuber KG, Dorsey JG, Tepperman K, Elder RC, (1995) Gold binding sites in red blood cells. *Inorg.Chim.Acta* 229: 271-280. doi: [http://dx.doi.org/10.1016/0020-1693\(94\)04254-S](http://dx.doi.org/10.1016/0020-1693(94)04254-S).

Additional online resource data

1) Molecular structure

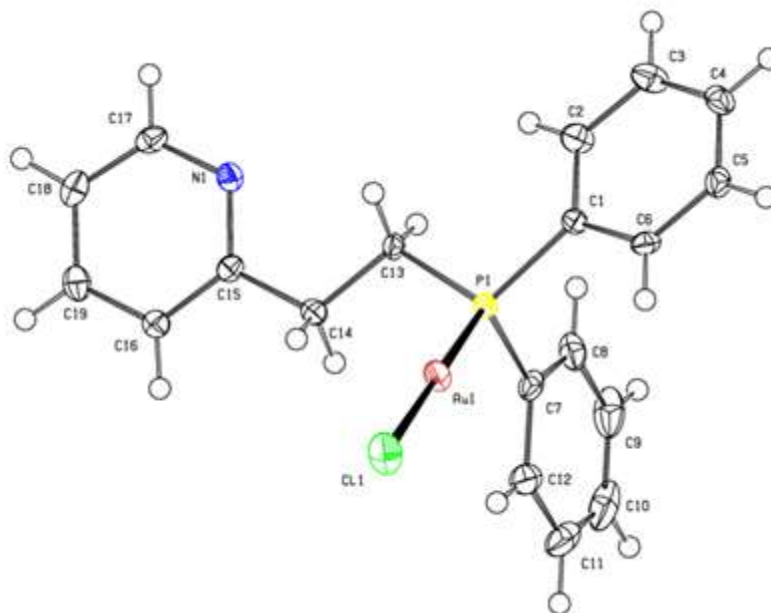


Fig S1: Molecular structure of **2** with 50% probability ellipsoids. The ORTEP diagram is presented for the purposes of showing the connectivity of the atoms. Hydrogen atoms and minor component of the disorder are omitted for clarity.

2) Crystal structure data information

Table SI: Crystallographic data for **2** and **1a**

Parameter	2	1a
Empirical formula	C ₁₉ H ₁₈ AuClNP	C ₂₂ H ₂₃ AuCl ₆ NPPdS
Formula weight	523.73	880.51
Temperature (K)	100(2)	100(1) K
Wavelength	0.71073 Å	0.71073 Å
Crystal system, space group	Monoclinic, P21/c	Monoclinic, P21/c
a (Å)	11.9075(11)	9.565(4)
b (Å)	12.0082(11)	17.495(6)
c (Å)	13.6018(12)	16.647(6)
α (°)	90	90
β (°)	114.160(2)	95.930(11)
γ (°)	90	90
Volume (Å ³)	1774.5(3)	2770.8(18)
Z	4	4
Density (calculated) (Mg/m ³)	1.960	2.111
Absorption coefficient (mm ⁻¹)	8.529	6.663
F(000)	1000	1680
Crystal size (mm ³)	0.32 x 0.06 x 0.02	0.40 x 0.20 x 0.20
Theta range for data collection (°)	1.87 to 28.40	1.69 to 33.28
Reflections collected	14352	71074
Completeness to theta = 28.40° %	99.3	99.0
R indices (all data)	R1 = 0.0317, wR2 = 0.0563	R1 = 0.0248, wR2 = 0.0461
Largest diff. peak & hole (e.Å ⁻³)	1.930 & -0.875	1.576 & -1.148

Table SII: Selected bond distances (Å) and angle (°) for **2**:

Bond distances (Å)		Bond angle (°)	
P-Au1	2.2368(8)		
Au1-Cl1	2.2972(9)	P1-Au1-Cl1	177.34(3)

3) Impedance profiles for 1 and 1a

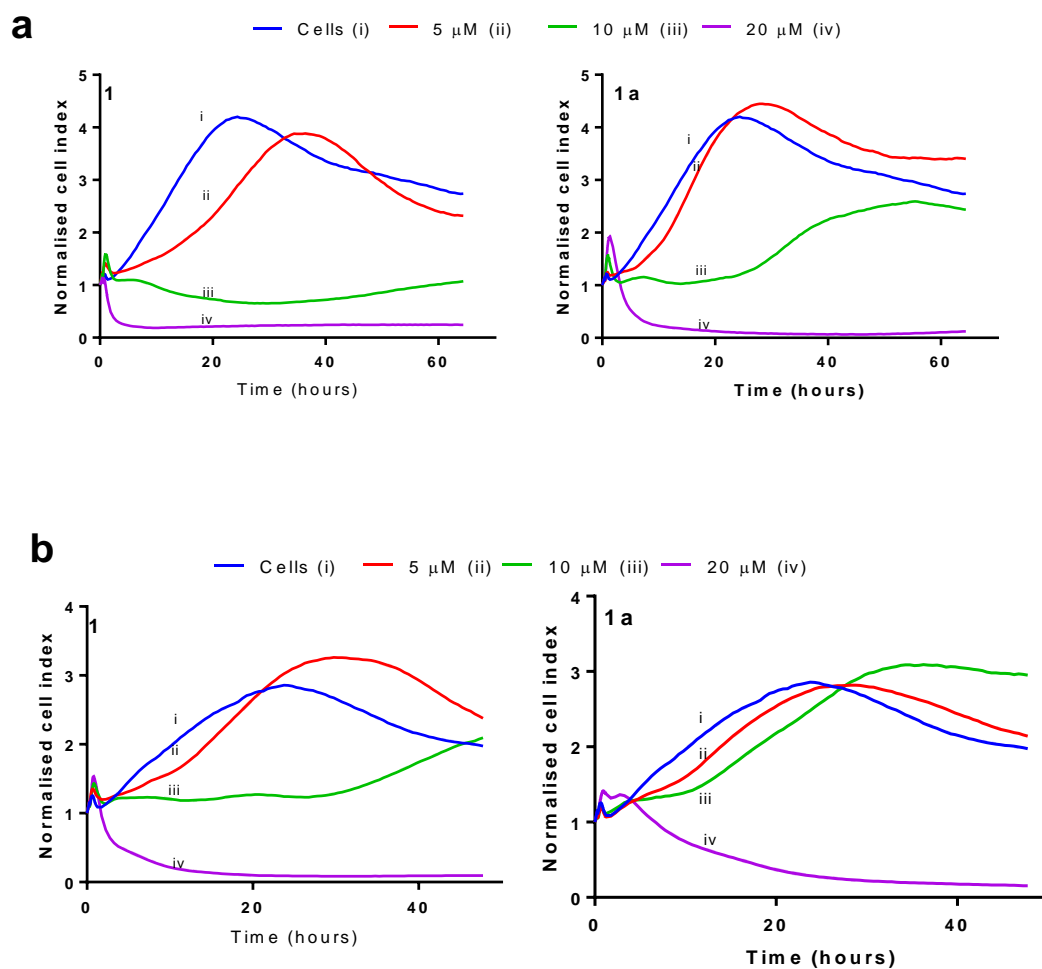


Fig SII: Repeat profiles for complex **1** and **1a**. A more rapid uptake of **1** (in a and b) at 20 μM is seen over **1a** (a and b). At 10 μM recovery was quicker for **1a** in both cases compared than for **1**. The impedance profile is represented as normalised cell index against time (h).

4) Impedance profile for 2

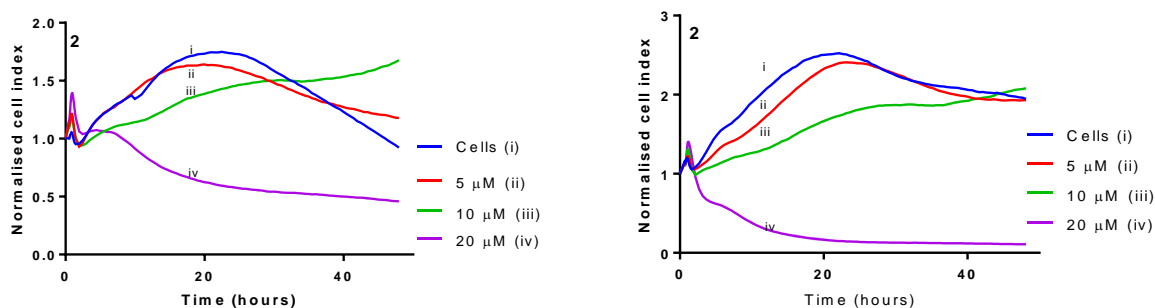


Fig SIII: Impedance proliferation profile of **2** at 5, 10 and 20 μM . A dose response profile was obtained.

5) Recovery pattern of complexes **1a** compared to **1** and **2**

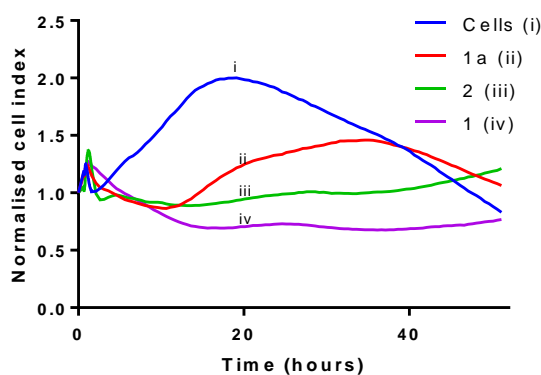
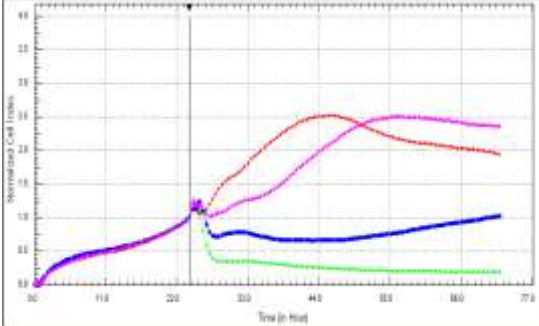


Fig SIV Recovery pattern of **1a** compared to **1** and **2** at 10 μM . Cells treated with **1a** recover quicker than those treated with **1** and **2**. Complex **1** is generally more toxic probably due to the absence of an ethyl group which is present in **2**. On the contrary, this group which is also absent in **1a** appears to be masked by the bimetallic entity which reduced the uptake of the later due to the non-ideal lipophilicity resulting in a less toxic bimetallic complex.

6) Comparative effect of cell viability proliferation and ADMET prediction of 2b

Table SIII:

	CC ₅₀ (μ M)	RT-CES profile	HIA	Aqueous solubility	Alogp98	Unknown AlogP98
2b	11.0 \pm 3.7		3	0	10.66	5